applied sciences

MDPI

Article

Green Synthesis, Characterization, and Antifungal Efficiency of Biogenic Iron Oxide Nanoparticles

Mohamed Taha Yassin *, Fatimah O. Al-Otibi, Abdulaziz A. Al-Askar and Raedah Ibrahim Alharbi

Botany and Microbiology Department, College of Science, King Saud University, Riyadh 11451, Saudi Arabia; falotibi@ksu.edu.sa (F.O.A.-O.); aalaskara@ksu.edu.sa (A.A.A.-A.); raalharbi@ksu.edu.sa (R.I.A.)
* Correspondence: myassin2.c@ksu.edu.sa

Abstract: The high incidence of fungal resistance to commercial fungicides and the negative effects of chemical fungicides on the environment and human health necessitate the development of novel biofungicides for the efficient management of fungal diseases. This study aims to greenly synthesize iron oxide nanoparticles (IONPs) using the aqueous extract of *Laurus nobilis* leaves and characterize these nanoparticles using various physicochemical techniques. The biogenic IONPs were tested against two pathogenic strains of *Alternaria alternata* and compared to the metalaxyl–mancozeb fungicide. The food poisoning technique was used to assess the antifungal efficacy of the greenly synthesized IONPs and the commercial metalaxyl–mancozeb fungicide against the tested pathogenic *A. alternata* strains. The biogenic IONPs showed a higher antifungal efficiency against the *A. alternata* OR236467 and *A. alternata* OR236468 strains at concentrations of 800 ppm compared to metalaxyl–mancozeb fungicide, with relative growth inhibition percentages of 75.89 and 60.63%, respectively. The commercial metalaxyl–mancozeb fungicide (800 ppm) showed growth inhibition percentages of 72.23 and 58.54% against the same strains. The biogenic IONPs also showed potential antioxidant activities against 1,1-diphenyl-2-picrylhydrazyl (DPPH) radicals, with DPPH inhibition percentages of 34.61% to 83.27%. In conclusion, the biogenic IONPs derived from *L. nobilis* leaves have the potential to be employed as biofungicides for the effective control of fungal phytopathogens, reducing reliance on harmful chemical fungicides.

Keywords: green synthesis; *Laurus nobilis*; characterization; antifungal; metalaxyl + mancozeb; antioxidant

Citation: Yassin, M.T.; Al-Otibi, F.O.; Al-Askar, A.A.; Alharbi, R.I. Green Synthesis, Characterization, and Antifungal Efficiency of Biogenic Iron Oxide Nanoparticles. *Appl. Sci.* **2023**, *13*, 9942. https://doi.org/10.3390/app13179942

Academic Editor: Solenne Fleutot

Received: 18 July 2023
Revised: 23 August 2023
Accepted: 29 August 2023
Published: 2 September 2023

1. Introduction

Fungi have been identified as the primary cause of significant reductions in crop yields across a wide range of agricultural produce. In developing countries, the situation is exacerbated, with fungal damage contributing to approximately 20–25% of overall production [1]. In contemporary times, the extent of fruit losses attributed to phytopathogenic fungi has been approximated to surpass 50% of the total agricultural fruit production [2]. Fungi are currently being recognized as emerging hazards to the health of animals, plants, and ecosystems [3]. Furthermore, the presence of fungal growth on food items can lead to the development of mycotoxicosis, a condition that arises from the consumption of mycotoxins. This can result in various severe manifestations, including acute poisoning, cancer, and liver diseases [4]. The occurrence of significant food waste has been attributed to the decomposition of fruits caused by fungal infections. Harvested fruits are susceptible to fungal attack due to factors such as abundant moisture, acidic pH, increased nutrient availability, and reduced intrinsic resistance [5]. Taking into account the reduction in crop productivity, *Alternaria* is identified as one of the most destructive saprophytic and pathogenic genera that impact matured and harvested vegetables and fruits [6]. Among the various species within this genus, *Alternaria alternata* has garnered significant attention in the academic literature due to its extensive documentation. Notably, this species has been found to possess

the capability of producing over 30 distinct mycotoxins [7]. *A. alternata* is responsible for inducing black spot rot on apple fruit and has the potential to generate various detrimental metabolites during its invasion [8]. Moreover, *A. Alternata* is known to produce non-host specific toxins, including alternariol monomethyl ether, alternariol, and tenuazonic acid, during its mycological growth. These toxins have the potential to posture a hazard to human health [9]. Furthermore, *A. Alternata* has been documented as a causative agent for several diseases, including citrus canker [10], core apple rot [11], Alternaria rot in nettled melon [12], and dragon fruit black rot [13]. In this context, *A. Alternata* fungus establishes its initial infection in the fruit via the peel or styles, typically through the growing period. Subsequently, it stays in a dormant condition until the fruit attains full maturity [14]. Various methodologies have been employed to manage the presence of *A. Alternata* in tomato crops [15]. Currently, the management of diseases relies on the application of agrochemicals, such as fungicides. Despite the numerous advantageous qualities of fungicides, such as their high availability, reliability, and fast action, it is important to acknowledge that these substances can have detrimental effects on non-target organisms [16]. The primary reason for their harmful effects is attributed to their toxic properties and their systemic mechanism of action, which interferes with the levels of metabolites in the biosynthesis pathway of aromatic amino acids in soil microorganisms. Moreover, it should be noted that these fungicides possess non-biodegradable properties, leading to their accumulation in water, soil, and plants. This accumulation subsequently results in detrimental consequences for other organisms within the ecosystem [17]. Additionally, the overuse of chemical fungicides can contribute to the development of fungal resistance, which in turn leads to a harmful impact on the environment [18]. Furthermore, it has been evaluated that approximately 80–90% of fungicides that are sprayed are subsequently lost to the environment either during or after their application [19]. Therefore, it is imperative to acquire fungicides that exhibit superior performance while remaining economically viable and minimizing adverse environmental effects.

Recently, various environmentally sustainable and highly effective alternatives have been suggested for the management of phytopathogenic fungi. These alternatives encompass the use of biological control methods [20], essential oils [21], plant extracts [22], and engineered nanomaterials [23]. The utilization of engineered nanomaterials has become increasingly significant in the management of phytopathogenic fungi due to their distinct physicochemical characteristics in comparison to their larger-scale counterparts [24]. As a result, several nanomaterials have demonstrated a superior efficacy compared to traditional agrochemicals in the management of plant diseases [25]. Various types of nanomaterials have been investigated as potential substitutes for the management of phytopathogenic fungi. These include carbon nanomaterials [26], nanopolymers [27], and metal nanoparticles [28–30]. Metal oxide nanoparticles have been widely recognized as a viable and environmentally sustainable option for managing phytopathogenic fungi in the field of agriculture [31,32]. Iron oxide nanoparticles (IONPs) have been recently utilized in various biotechnological applications. These include the immobilization of enzymes on multifunctional magnetic nanomaterials [33], the development of low-cost biosensors for the detection of pathogenic bacteria using graphene-magnetic@chitosan nanosheets [34,35], and biomedical applications [36].

In this context, IONPs were reported to possess antifungal effectiveness against fungal phytopathogens [37,38]. A previous study indicated that the biogenic iron oxide nanoparticles of *Euphorbia helioscopia* leaf extract were spherical in shape, where the particle size ranged from 7 to 10 nm and possessed antifungal efficiency against the *Cladosporium herbarum* strain [39]. The prevalence of fungal resistance has been widely observed and is primarily attributed to the excessive utilization of chemical fungicides. In addition to their detrimental effects on the environment, the urgent need for alternative fungicides that can be safely applied has become apparent. Therefore, the present study was conducted to greenly synthesize IONPs utilizing aqueous *Laurus nobilis* leaf extract. Additionally, the biosynthesized IONPs were characterized via the application of physicochemical tech-

niques. Furthermore, the efficacy of the IONPs was assessed in terms of their antifungal properties. This evaluation was conducted using a food poisoning technique, specifically targeting the pathogenic *A. alternata* strain known to cause significant damage to matured and harvested vegetables and fruits. Furthermore, a comparison was made between the antifungal effectiveness of the phytosynthesized IONPs and a commercially available fungicide known as metalaxyl + mancozeb fungicide to determine the possible applicability of the biogenic IONPs in controlling phytopathogenic fungi.

2. Materials and Methods

2.1. Preparation of L. nobilis Extract

The dry leaves of *Laurus nobilis* were acquired from a local market situated in Riyadh, Saudi Arabia. The verification of the plant specimens' identification was affirmed via the herbarium housed within the department of Botany and Microbiology. The dried leaves of *L. nobilis* underwent a triple purification procedure utilizing distilled water subsequent to a preliminary rinse with tap water. Following this, they were allowed to undergo complete drying in the ambient atmosphere. The leaves were pulverized into a homogeneous and finely powdered powder using a mechanical blender. A flask with a volume of 500 mL was used to hold a quantity of 50 g of plant powder together with 200 mL of distilled water. The flask was subjected to a temperature of 60 °C for 30 min using a hot plate. The flask was subsequently exposed to continuous agitation for a duration of 24 h at 25 °C, facilitated via the utilization of a magnetic stirrer. Afterwards, the mixture underwent purification by means of Whatman filter paper (1) in order to obtain a purified filtrate and remove any remaining substances. Subsequently, the extract underwent sterilization via filtration using a 0.45 μm Millipore membrane filter. Subsequently, the prepared extracts were subjected to refrigeration at a temperature of 4 °C in order to preserve them for subsequent experiments.

2.2. Green Biofabrication of IONPs

For the biosynthesis of IONPs, a solution containing 0.01 M of Ferric nitrate ($Fe(NO_3)_3 \cdot 9H_2O$) was added to the aqueous extract of *L. nobilis* in a 1:1 ratio. The observation of a dark brown color suggested the formation of IONPs. The reduced solution was subjected to centrifugation at 10,000 rpm for 10 min. Following centrifugation, the supernatant was removed and discarded. The pellets underwent a triple washing process using distilled water in order to eliminate any impurities [40].

2.3. Physicochemical Characterization of the Biogenic IONPs

Various techniques were employed to characterize the biogenic IONPs, including UV-Vis spectroscopy, which was utilized to determine the optical properties of the IONPs. The shape and particle size distribution of the biosynthesized IONPs were examined utilizing a Transmission Electron Microscope (TEM) (model JEM1011, JEOL, Tokyo, Japan). Furthermore, the elemental composition of IONPs was determined via the utilization of an Energy-Dispersive X-ray (EDX) analysis. Additionally, a Fourier transform infrared spectroscopy (FTIR) analysis was employed to identify the primary functional groups present in the biofabricated IONPs. The biogenic IONPs underwent a X-ray powder diffraction (XRD) examination to affirm their crystalline structure and detect their crystalline size. The Zeta sizer instrument (Malvern Instruments Ltd.; zs90, Worcestershire, UK) was utilized to assess the zeta potential value and hydrodynamic diameter of IONPs.

2.4. Antifungal Efficiency of Standard Fungicide against the Tested Strains

Two pathogenic strains of *Alternaria alternata*, namely *A. alternata* OR236467 and *A. alternata* OR236468 were provided from the Botany and Microbiology Department, College of Science, King Saud University. The food poisoning method was employed to assess the antifungal effectiveness of a commercially available fungicide, specifically (Metalaxyl + Mancozeb), against the fungal strains under investigation. Various concentrations of the fungicide (50, 100, 200, 400, and 800 ppm) were introduced into the PDA

medium subsequent to the process of sterilization. Subsequently, the plates were inoculated with a 6 mm disc containing fungal growth and subjected to incubation at a temperature of 25 ± 2 °C for a duration of 7 days. In contrast, control PDA plates were utilized, which were inoculated solely with a 6 mm disc of fungal growth. The measurement of the growth diameter of the pathogenic fungal strain was conducted utilizing a Vernier caliper. The growth inhibition ratio (%) was determined by applying the following formula:

$$\% \text{ inhibition} = (A - B)/A \times 100$$

where A represents the growth diameter observed in the control plates, and B represents the growth diameter observed in the treated plates.

2.5. Antifungal Effectiveness of the Biogenic IONPs against the Tested Fungal Strain

The antifungal efficacy of the biogenic IONPs was assessed using the food poisoning method against the tested fungal pathogens under investigation. Different concentrations of the biogenic IONPs (50, 100, 200, 400, and 800 ppm) were introduced into the PDA medium after sterilization. Following this, the plates were inoculated with a 6 mm disc containing fungal growth and placed in an incubator set at a temperature of 25 ± 2 °C for a period of 7 days. On the other hand, control PDA plates were employed, wherein only a 6 mm disc of fungal growth was inoculated. The diameter of the pathogenic fungal strain was measured using a Vernier caliper. The calculation of the growth inhibition ratio (%) was performed utilizing the following formula: % inhibition = (A − B)/A × 100. In this equation, A represents the growth diameter observed in the control plates, while B represents the growth diameter observed in the treated plates.

2.6. Antioxidant Assay

A 1,1-diphenyl-2-picrylhydrazyl (DPPH) assay was conducted to assess the efficacy of the biogenic IONPs in scavenging the free radicals. Different concentrations (50, 100, 150, 200, and 250 mg/mL) of the biogenic IONPs were prepared using methanol as the solvent. A 1 mM solution of DPPH was prepared by dissolving it in 100 mL of methanol. A 2 mL aliquot of DPPH solution was mixed with the biogenic iron oxide nanoparticles of varying concentrations. The solution was subjected to incubation at ambient temperature for 30 min under dark conditions. Ascorbic acid was used as a positive control, whereas an equal amount of methanol and DPPH was used as a blank. The absorbance of the reaction mixtures at a wavelength of 517 nm was measured using a UV spectrophotometer, and the percentage of inhibition was calculated using the following equation:

$$\% \text{ DPPH scavenging} = [(A - B)/A] \times 100,$$

whereas A is the absorbance of the control and B is the sample absorbance [41].

2.7. Statistical Analysis

The data in the current research were analyzed using GraphPad Prism version 8.0 (GraphPad Software, Inc., La Jolla, CA, USA) by the use of the Tukey test in a One-way ANOVA, with the significance level set at 0.05. The data were reported in the form of the mean of triplicates accompanied by the standard error.

3. Results and Discussion

3.1. Green Biosynthesis of IONPs

The aqueous extract derived from the leaves of *L. nobilis* was employed in the environmentally friendly synthesis of iron oxide nanoparticles (IONPs), as depicted in Figure 1. The plant extract derived from *L. nobilis* demonstrates the capability to function as a reducing agent for the ferric nitrate solution, leading to the formation of IONPs. Figure 1A illustrates the utilization of *L. nobilis* leaf extract as a reducing agent for the ferric nitrate solution (Figure 1B), resulting in a change from a yellowish-orange color to the formation of

dark brown-colored IONPs (Figure 1C). In this particular context, it has been reported that the aqueous extract derived from the leaves of *L. nobilis* contains a diverse range of bioactive constituents, such as phenolic compounds, alkaloids, saponins, flavonoids, tannins, glucosides, steroids, and proteins [42]. The generation of iron nanoparticles is ascribed to the influence exerted by these phytochemicals [43]. The aqueous leaf extract fulfills a dual role in the process of nanoparticle synthesis. Initially, it serves as a reducing agent for the solution of ferric nitrate, thereby facilitating the formation of IONPs. Additionally, it functions as a stabilizing agent, hindering the aggregation of the synthesized nanoparticles [44]. Various techniques were used to assess the physicochemical characteristics of the biosynthesized IONPs.

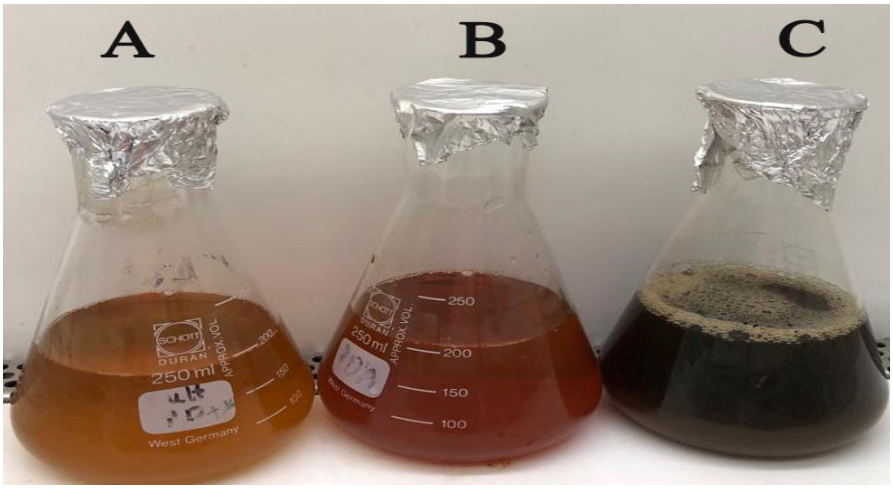

Figure 1. Green synthesis of IONPs utilizing aqueous extract of *L. nobilis*. (**A**): water leaf extract of *L. nobilis*, (**B**): ferric nitrate solution, (**C**): the biogenic IONPs.

3.2. UV Analysis of the Phyto-Synthesized IONPs

The UV-Visible spectrum was analyzed for the aqueous extract of *L. nobilis* leaves and the biogenic IONPs in order to identify the surface plasmon resonance (SPR) of the biogenic IONPs. Figure 2A illustrates the emergence of a wide spectral peak ranging from 330 to 360 nm, which may be attributed to the presence of phytochemical compounds inside the plant extract. However, the UV-Visible spectrum of the biogenic IONPs exhibited the presence of a wide peak spanning from 385 to 400 nm, indicating the occurrence of SPR in the biogenic IONPs, as seen in Figure 2B. The results of our study align with those of prior research, which demonstrated that the UV spectral data showed the presence of a peak at 379 nm, indicating the formation of the biogenic IONPs derived from *Eichhornia crassipes* leaf extract [45].

3.3. EDX Analysis of the Biogenic IONPs

The elemental composition of IONPs was determined via the utilization of EDX analysis. The biosynthesized IONPs consisted of four elements: iron, oxygen, carbon, and silicon. These elements were present in the IONPs with mass percentages of 53.78%, 21.51%, 16.56%, and 8.15%, respectively (Figure 3). The peaks corresponding to iron were observed at signals of 0.8, 6.4, and 7.0 keV for Fe La, Fe Ka, and Fe Kb, respectively. Conversely, the signals detected at signals of 0.3, 0.5, and 1.7 keV were attributed to carbon (C), oxygen (O), and silicon (Si), respectively. The observed signal of silicon could be attributed to the presence of capping molecules derived from the extract of *L. nobilis* leaves [46]. In the present context, the observed percentage of iron was found to be greater than that reported in a prior study. The previous investigation revealed that the biogenic IONPs produced using tea pruning waste exhibited a weight percentage of 51.79% [47]. This finding suggests that the biosynthesis method utilizing *L. nobilis* extract is highly effective. Figure 4 shows a SEM graph of the IONPs formulated using *L. nobilis* leaf extract.

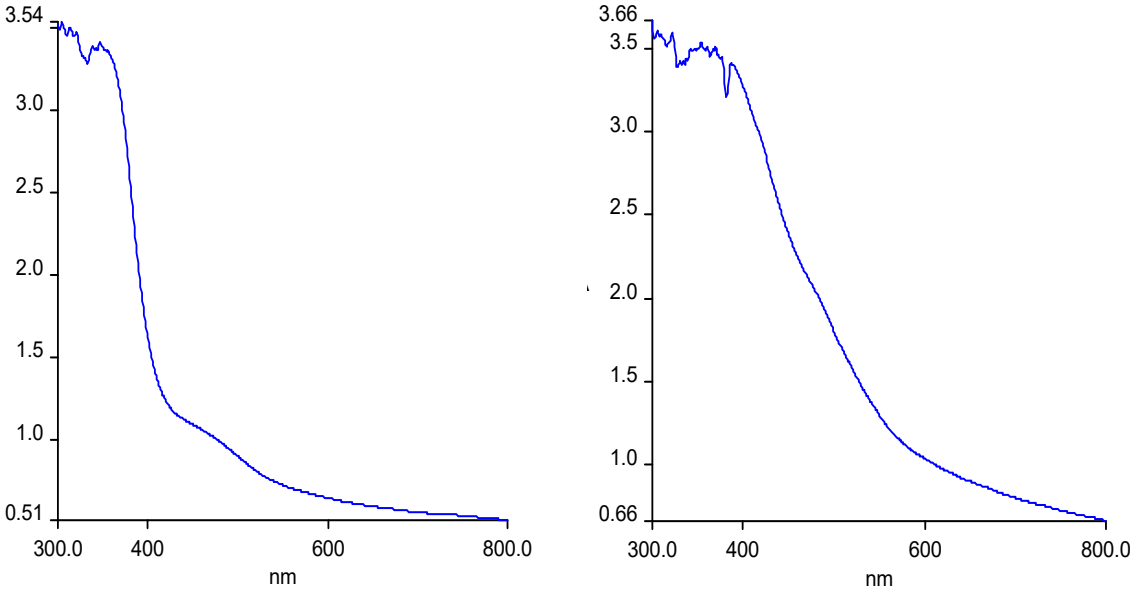

Figure 2. (**A**): UV-Vis spectrum of *L. nobilis* leaf extract; (**B**): UV-Vis spectrum of the biogenic IONPs).

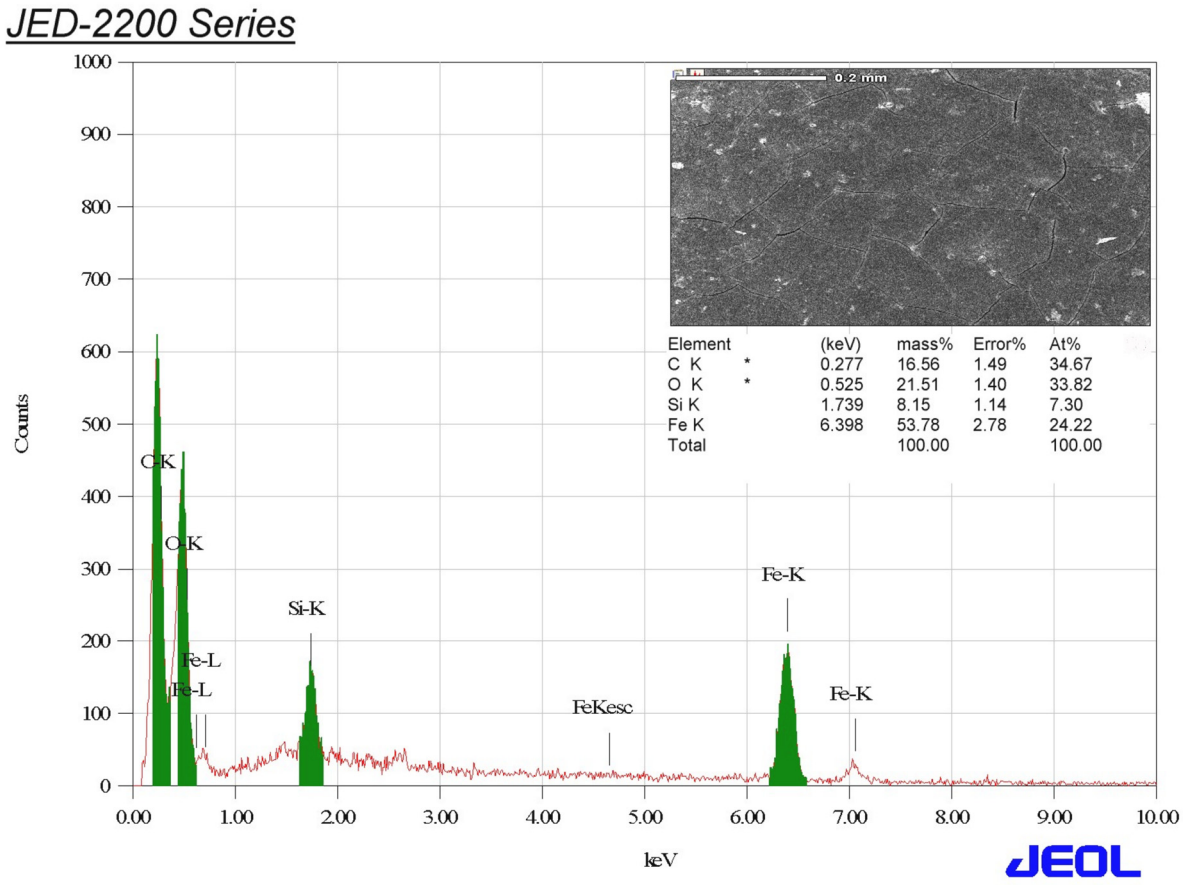

Figure 3. EDX analysis of the biogenic IONPs.

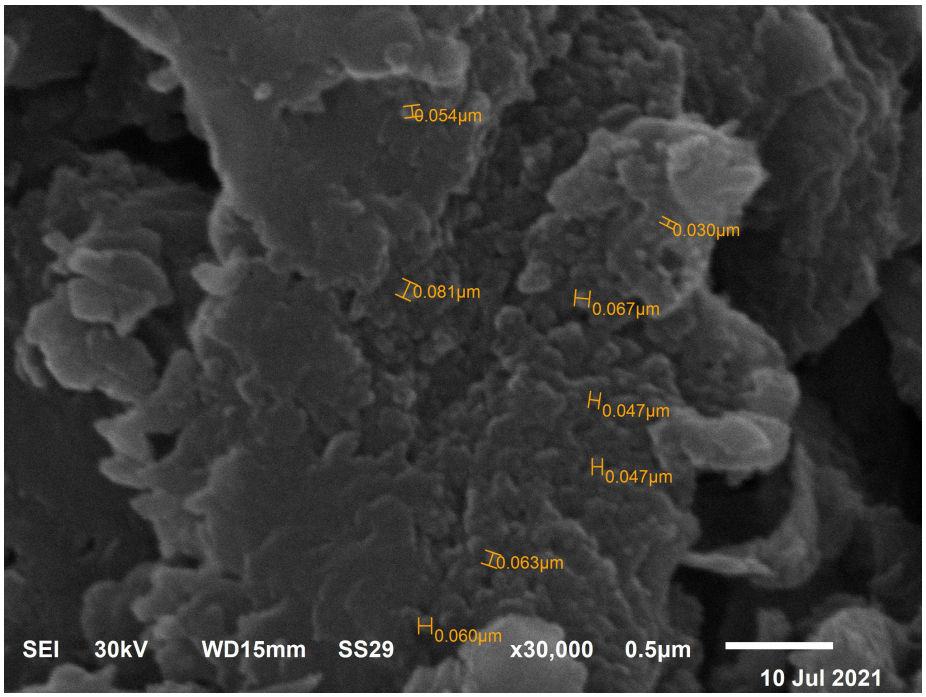

Figure 4. SEM image of the biogenic IONPs.

3.4. FTIR Analysis of the Biogenic Fe_2O_3 Nanoparticles

Fourier-transform infrared (FT-IR) spectroscopy was used to analyze the surface chemical composition and functional groups of the biogenic IONPs, as well as to investigate any potential surface interactions [48]. The FTIR spectrum of the aqueous leaf extract of *L. nobilis* demonstrated the presence of six absorption bands at 3427.08, 2927.22, 2847.61, 1632.01, 1030.37, and 540.36 cm^{-1}, whereas the FTIR spectrum of the biogenic IONPs demonstrated the presence of eight absorption bands at 3434.74, 2921.47, 1621.34, 1444.05, 1352.94, 1176.47, 1075.45, and 574.83 cm^{-1} (Figure 5). In this context, the O-H stretching was observed in the spectrum of the aqueous extract of *L. nobilis* at a wavenumber of 3427.08 cm^{-1}, providing evidence for the existence of alcoholic and phenolic functional groups. The prominent peak seen at 3434.74 cm^{-1} in the FTIR spectrum of the biogenic IONPs might be ascribed to the stretching vibration of the O-H bond in phenolic compounds that are adsorbed onto the nanoparticle surface during the synthesis process [49]. The spectral analysis of the *L. nobilis* extract revealed the presence of two distinct bands at 2927.22 and 2847.61 cm^{-1}. These bands may be attributed to the stretching of C-H bonds in alkanes. The functional groups of alkanes present in the extract may have been capped on the surface of the biogenic IONPs, as shown by the detection of a band at a wavenumber of 2921.47 cm^{-1} [50,51]. The absorption bands seen at wavenumbers of 1632.01 and 1621.34 cm^{-1} in the spectra of *L. nobilis* and the biogenic IONPs might be ascribed to the N-H bending of amine functional groups that are capped over the surface of the biogenic IONPs, as suggested by previous research [52]. Moreover, the absorption band located at 1444.05 cm^{-1}, might be attributed to the C-C stretching of aromatic C=C [53]. Moreover, the band noticed at 1352.94 cm^{-1} could be ascribed to the O-H bending of phenolics [54]. In addition, the band observed at 1176.47 cm^{-1} might be assigned to the C-N stretching of amines. However, the absorption band detected at 1030.37 cm^{-1} of the extract might be ascribed to the COO- carbonyl group [55]. Similarly, the band seen at a wavenumber of 1075.45 cm^{-1} in the biogenic IONPs may be attributed to the stretching of C-O bonds present in alcoholic functional groups (Table 1) [56]. Finally, the characteristic transmission bands detected at 540.36 and 574.83 cm^{-1} were assigned to the alkyl halides as previously reported [57]. Collectively, FTIR analysis affirmed that the phenols, alcohols, amines, and

alkanes of the plant extract act as reducing, stabilizing, and capping agents for the biogenic IONPs.

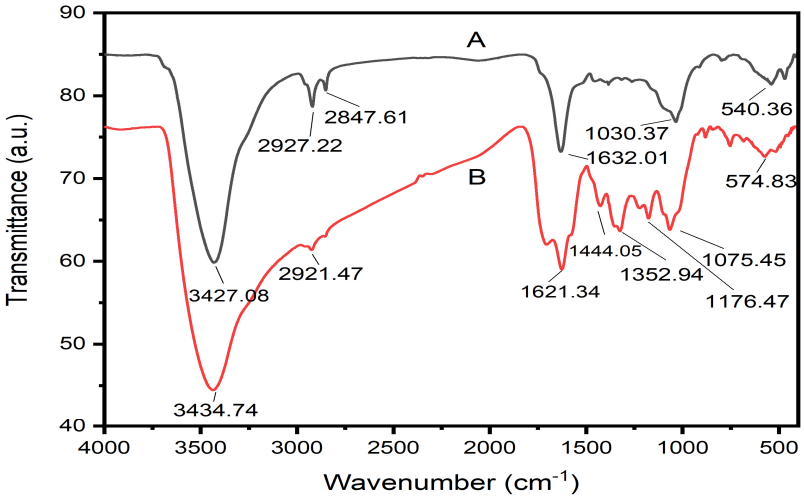

Figure 5. FTIR spectrum of *L. nobilis* leaf extract and the biogenic IONPs (A: FTIR spectrum of *L. nobilis* extract; B: FTIR spectrum of the biogenic IONPs).

Table 1. Functional groups of the *L. nobilis* leaf extract and the biogenic IONPs.

Functional Groups of the Aqueous Leaf Extract of *L. nobilis*				
No.	**Absorption Peak (cm^{-1})**	**Appearance**	**Functional Groups**	**Molecular Motion**
1	3427.08	Strong, broad	Phenols	O-H stretching
2	2927.22	Medium	Alkanes	C-H stretching
3	2847.61	Medium	Alkanes	C-H stretching
4	1632.01	Medium	Amines	N-H bending
5	1030.37	Medium	Carbonyl groups	C-O stretching
6	540.36	Weak, broad	Alkyl halides	C-Br stretching
Functional groups of the biogenic IONPs				
1	3434.74	Strong, broad	Phenols	O-H stretching
2	2921.47	Medium	Alkanes	C-H stretching
3	1621.34	Medium	Amines	N-H bending
4	1444.05	Medium	Aromatic compounds	C-C stretching
5	1352.94	Medium	Phenols	O-H bending
6	1176.47	Medium	Amines	C-N stretching
7	1075.45	Medium	Primary alcohols	C-O stretching
8	574.83	Weak, broad	Alkyl halides	C-Br stretching

3.5. TEM Investigation of IONPs

Iron oxide nanoparticles were investigated using TEM analysis for the determination of the shape, size and particle size distribution of the phytosynthesized IONPs. In this context, the biogenic IONPs were observed to be embedded within a matrix-like structure, which could be assigned to the biomolecules of *L. nobilis* leaf extract utilized in the biosynthesis procedure, as shown in Figure 6 [58]. The biogenic iron oxide nanoparticles exhibited a spherical morphology, with an average particle size of 46.3 nm (Figure 7).

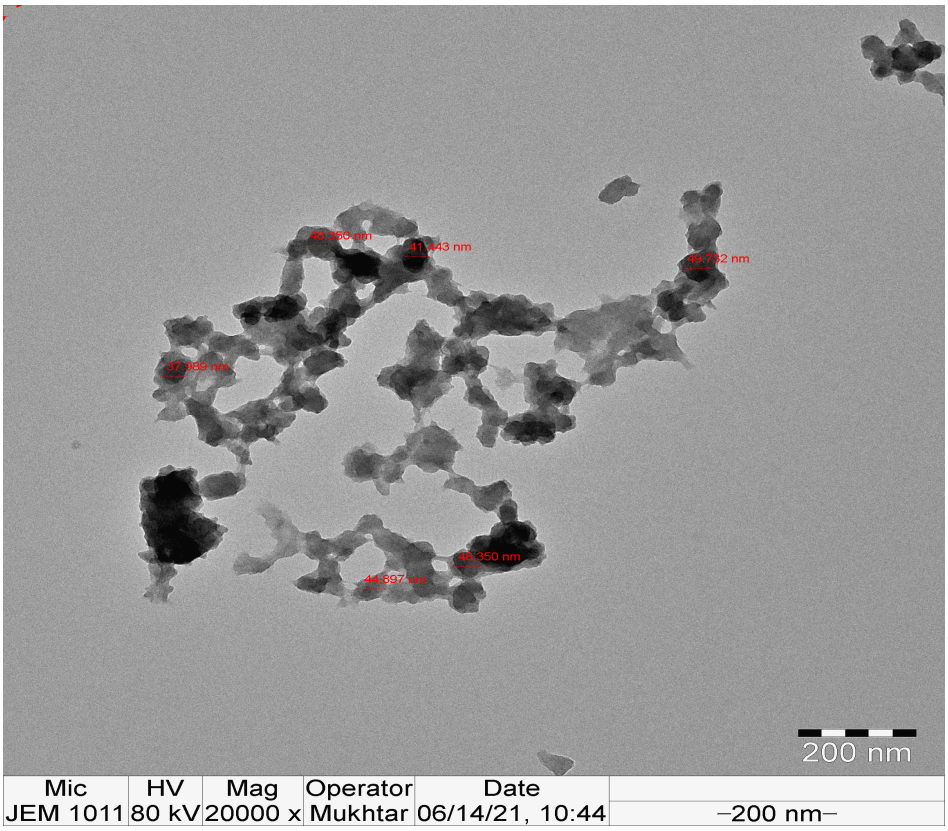

Figure 6. TEM image of the phytosynthesized Fe_2O_3 nanoparticles.

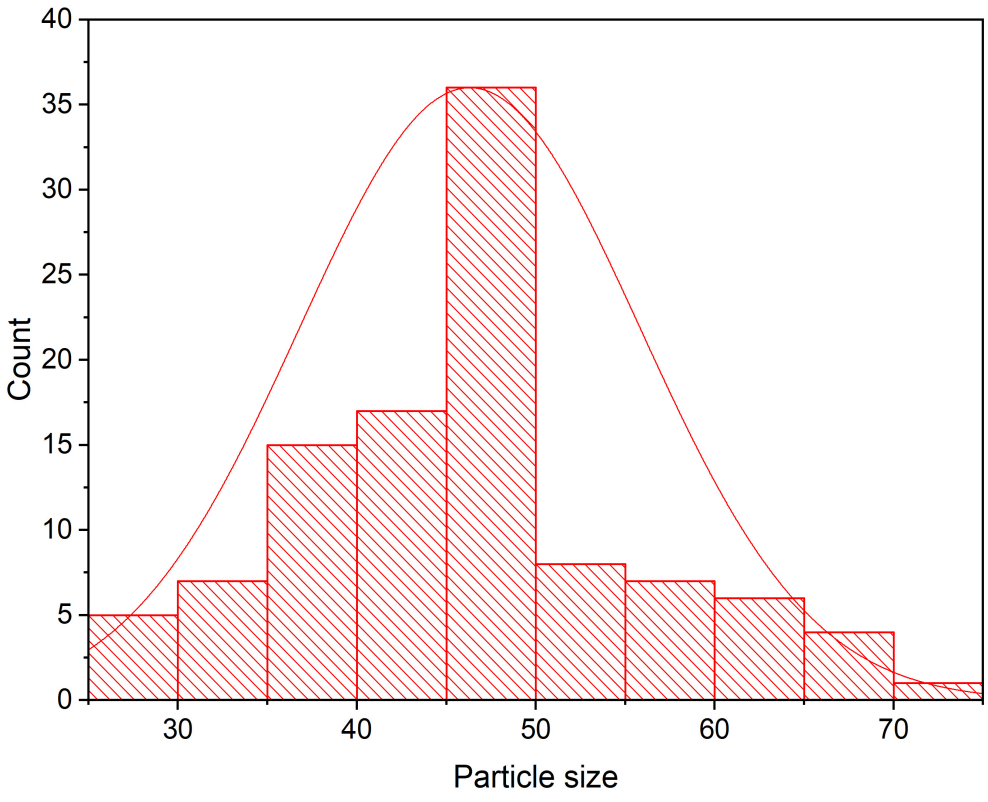

Figure 7. Particle size distribution of the phytosynthesized IONPs.

3.6. XRD Analysis of the Biogenic IONPs

The X-ray powder diffraction analysis was employed to characterize the crystalline structure and identify the phase of the nanoparticles. XRD analysis, as depicted in Figure 8, indicates that the synthesized nanoparticles possess distinct and sharp peaks. This observation suggests that the nanoparticles exhibit a high degree of crystallinity and closely align with the established reference values for the hexagonal rhombohedral α-Fe_2O_3 phase (JCPDS-33-0664). In addition, the synthesized nanoparticles exhibit characteristics that classify them as photocatalysts due to the presence of distinct and intense peaks at 2θ values of 33.2 and 35.6°. These peaks correspond to the preferential orientations along the (104) and (110) crystallographic planes, respectively [59]. The XRD pattern demonstrated the presence of ten diffraction peaks at two theta degrees of 24.52, 33.52, 35.62, 40.53, 49.44, 57.78, 62.74, 64.35, and 71.64°, corresponding to the lattice planes of (012), (104), (110), (113), (024), (116), (018), (214), (300), and (010), respectively (Figure 7). These results were consistent with those of prior studies [59–61]. The crystalline grain size of the biogenic Fe_2O_3 was detected according to Scherrer's formula as follows: L = Kλ/β. cos θ, whereas K is Scherrer's constant (0.94), ω is the X-ray wavelength (for copper, λ = 1.5406 Å), and β is the full width at the half-maximum (FWHM) of the most intense peak at 2θof 33.52°, which was found to be 0.1824. The estimated crystalline size of the phytosynthesized IONPs was found to be 47.59 nm.

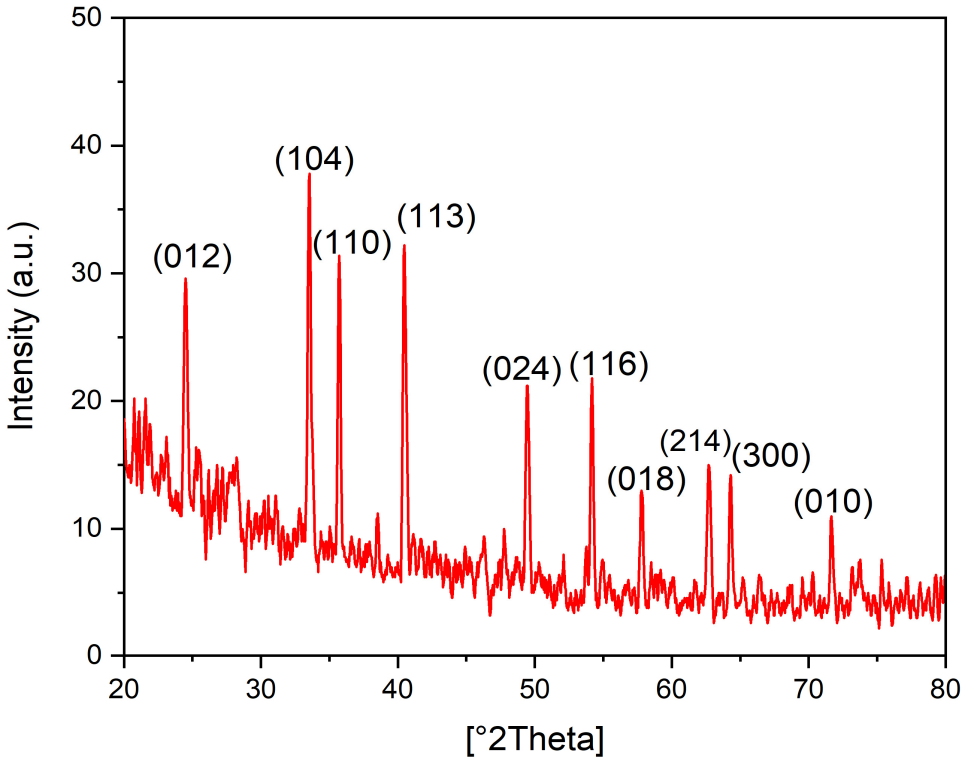

Figure 8. XRD pattern of the biogenic IONPs synthesized using *L. nobilis* leaf extract.

3.7. Zeta Potential Analysis

The present study used dynamic light scattering (DLS) analysis to determine the average hydrodynamic diameter of the biogenic IONPs synthesized using an extract derived from *L. nobilis* leaves. In this context, the hydrodynamic diameter was ascertained to be 312.6 nm (Figure 9), indicating a greater magnitude in comparison to the measurements acquired via TEM and XRD methodologies. The observed difference may be ascribed to the inclusion of the size estimate for the biogenic IONPs nanoparticles, together with the consideration of capping biomolecules and the surrounding hydrate layers in the DLS analysis [62]. Moreover, the zeta potential value of the phytosynthesized IONPs was detected to be −11.6 mV (Figure 10). The surface negative charge of IONPs might be allotted to

the extract biomolecules. A previous investigation indicated that *Rhamnella gilgitica* leaves revealed a zeta potential charge of −8.7 mV [63].

			Size (d.nm):	% Intensity:	St Dev (d.n...
Z-Average (d.nm):	312.6	Peak 1:	455.0	100.0	73.43
PdI:	0.235	Peak 2:	0.000	0.0	0.000
Intercept:	0.706	Peak 3:	0.000	0.0	0.000
Result quality :	Refer to quality report				

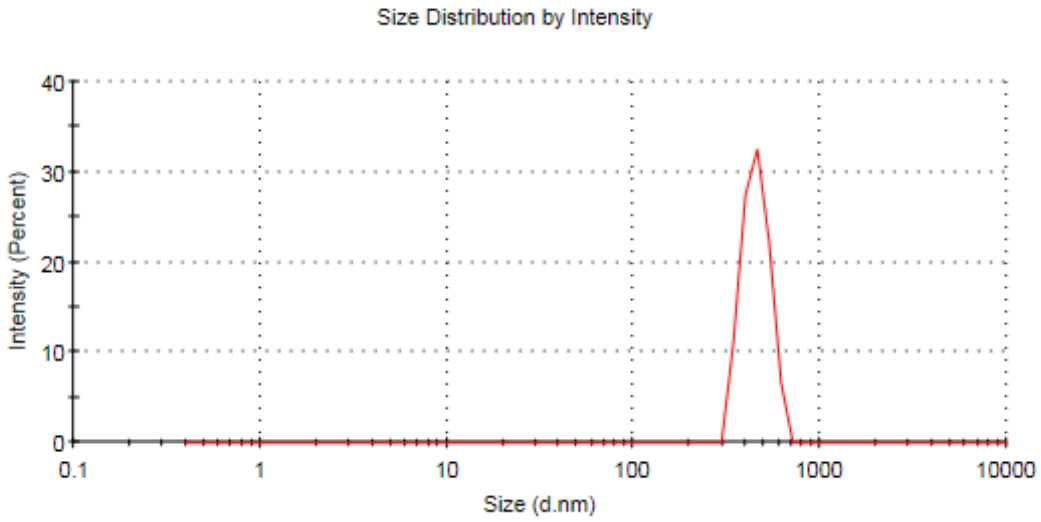

Figure 9. The average hydrodynamic diameter of the biogenic Fe_2O_3 nanoparticles.

			Mean (mV)	Area (%)	St Dev (mV)
Zeta Potential (mV):	-11.6	Peak 1:	-11.6	100.0	5.36
Zeta Deviation (mV):	5.36	Peak 2:	0.00	0.0	0.00
Conductivity (mS/cm):	0.111	Peak 3:	0.00	0.0	0.00
Result quality :	Good				

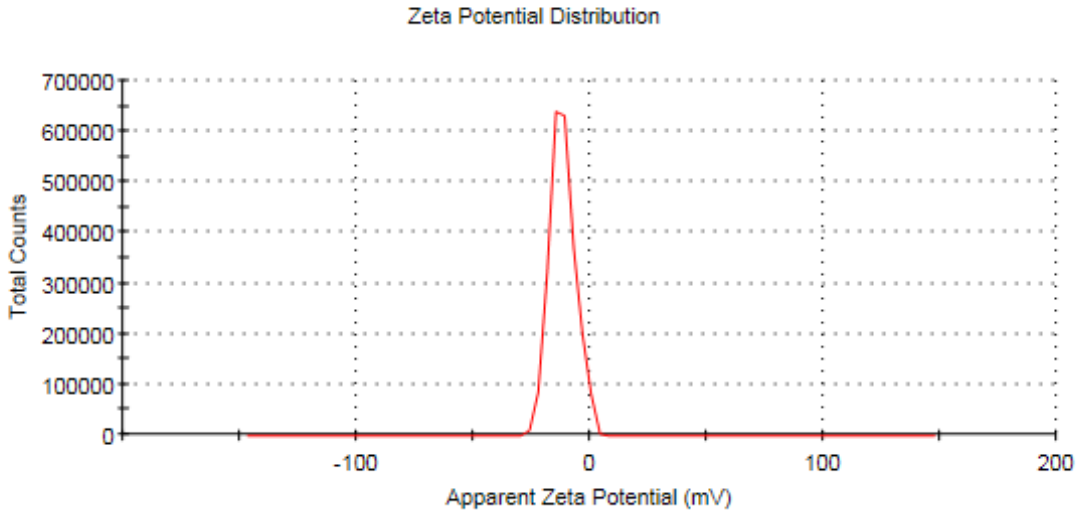

Figure 10. The surface charge of the phytosynthesized Fe_2O_3 nanoparticles.

3.8. Antifungal Efficacy of Standard Fungicide and Biogenic Iron Oxide Nanoparticles Against

Different concentrations of the biogenic iron oxide nanoparticles (50, 100, 200, 400, and 800 ppm) were evaluated for their antifungal activity against the *A. alternata* OR236467 and *A. alternata* OR236468 strains utilizing the food poisoning technique (Figure 11). The commercial fungicide, namely, metalaxyl + mancozeb, at the concentration of 800 ppm revealed a higher antifungal efficiency against the *A. alternata* OR236467 strain compared to the *A. alternata* OR236468 strain, demonstrating relative growth inhibition percentages of 72.23 and 58.54%, respectively. Accordingly, the *A. alternata* OR236468 strain showed a high resistance to the metalaxyl + mancozeb fungicide compared to the *A. alternata* OR236467 strain. The antifungal efficiency of the biogenic IONPs synthesized using *L. nobilis* extract (800 ppm) revealed a higher antifungal efficiency compared to the metalaxyl + mancozeb fungicide against the *A. alternata* OR236467 strain, demonstrating relative growth inhibition percentages of 75.89 and 72.23%, respectively (Tables 2 and 3). Interestingly, the *A. alternata* OR236468 strain revealed a higher level of susceptibility to the phytosynthesized IONPs in all of the tested concentrations compared to the metalaxyl + mancozeb fungicide. In the present study, the *A. alternata* OR236468 strain exhibited a fungal growth diameter of 24.31 ± 0.18 mm when exposed to a concentration of 800 ppm of the biogenic IONPs. This measurement was found to be significantly lower than the control, which had a fungal growth diameter of 58.63 ± 0.43 mm. These results suggest that the biogenic IONPs are highly effective in inhibiting the growth of the tested strain, surpassing the efficacy of the metalaxyl + mancozeb fungicide. Furthermore, the fungal growth strain *A. alternata* OR236467 exhibited a significant inhibition when subjected to treatment with the biogenic IONPs, as compared to the control group. Within this particular context, it is observed that the growth diameter experiences a reduction, specifically from a diameter of 78.35 ± 0.16 mm in the control group to a diameter of 18.89 ± 0.78 mm in the treatment group, subjected to 800 ppm of the biogenic IONPs. Collectively, the antifungal bioactivity of the biogenic IONPs was found to increase with the increasing concentration. The findings of our study align with those of a previous investigation that assessed the antifungal efficacy of the biogenic IONPs of *Oscillatoria limnetica* using the food poisoning technique. The prior report revealed that the higher concentrations of the biogenic IONPs exhibited a higher impact on the growth of fungal mycelium, with the greatest inhibition percentage observed at a concentration of 200 µg/mL of the biogenic IONPs [64]. The biogenic IONPs synthesized using the leaf extract of *Parthenium hysterophorus* were reported to possess antifungal effectiveness against the *Aspergillus niger* and *A. flavus* strains [65]. Moreover, the antifungal efficiency of the biogenic IONPs synthesized using *Chlorella*-K01 extract was confirmed against *Fusarium oxysporum*, *Fusarium maniliforme*, *Fusarium tricinctum*, *Rhizoctonia solani*, and *Phythium* sp. [66]. Furthermore, the phyto-synthesized IONPs of *Laurus nobilis* L. leaf extract revealed antifungal efficiency against the *Aspergillus flavus* and *Penicillium spinulosum* strains [67]. Another study affirmed the antifungal efficiency of IONPs of *Euphorbia herita* leaf extract at a concentration range from 10 to 30 mg/mL against the *Aspergillus fumigatus*, *Aspergillus niger*, and *Arthogrophis cuboida* strains [68]. Collectively, the biogenic IONPs synthesized using *L. nobilis* extract was found to possess a potential antifungal efficiency at low concentrations of 50 and 100 ppm comparable to previous reports, indicating their potential use as natural fungicides, avoiding the harmful impact of synthetic chemical fungicides. Interestingly, the phytosynthesized IONPs revealed a higher antifungal efficiency against the tested strain compared to the commercial fungicide of metalaxyl + mancozeb at low concentrations of 50 and 100 ppm, indicating their possible application of these nanoparticles as alternative to the chemically synthesized fungicides and avoiding their harmful impact on the environment [69]. Furthermore, the utilization of the biogenic IONPs presents a potential solution to address the issue of fungal resistance resulting from the excessive application of chemical fungicides [70,71]. A prior investigation has provided evidence that the first stage in which the biogenic IONPs exhibit antifungal effectiveness is attributed to their disruption of the cell envelope, which plays a crucial function in fungal cells. The presence of antimicrobial interaction might lead to

the elimination or functional inefficiency of the cytoplasmic membrane. The disruption of microbial membranes is attributed to the release of micro ions, namely potassium and phosphate radicals, along with larger molecules such as RNA, DNA, and other intracellular substances [72].

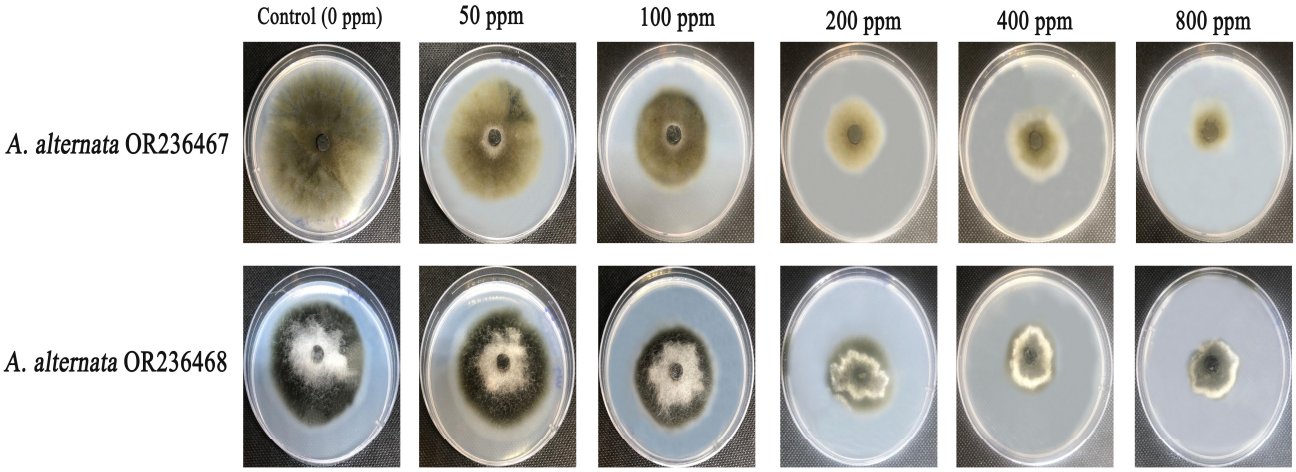

Figure 11. The effect of different concentrations of biogenic iron oxide nanoparticles against the two tested *A. alternata* strains.

Table 2. Growth inhibition percentages of different concentrations of metalaxyl + mancozeb against the tested *A. alternata* strains.

Fungicide Metalaxyl + Mancozeb (ppm)	Fungal Growth Diameter (mm)		Growth Inhibition Percentage (%)	
	A. alternata OR236467	*A. alternata* OR236468	OR236467	OR236468
Control (0 ppm)	78.67 ± 0.11 ^{a}	58.63 ± 0.43 ^{a}	0.00 ^{a}	0.00 ^{a}
50	67.23 ± 0.54 ^{b}	54.14 ± 0.32 ^{b}	14.54 ^{b}	7.65 ^{b}
100	58.16 ± 0.42 ^{c}	46.53 ± 0.29 ^{c}	26.07 ^{c}	20.64 ^{c}
200	43.17 ± 0.61 ^{d}	38.12 ± 0.49 ^{d}	45.13 ^{d}	34.98 ^{d}
400	30.64 ± 0.17 ^{e}	30.48 ± 0.15 ^{e}	61.05 ^{e}	48.01 ^{e}
800	21.85 ± 0.31 ^{f}	24.31 ± 0.18 ^{f}	72.23 ^{f}	58.54 ^{f}

Different letters in the same column indicated that values were significantly different at $p \leq 0.05$.

Table 3. Growth inhibition percentages of different concentrations of iron oxide nanoparticles against the two tested *A. alternata* strains.

IONPs (ppm)	Fungal Growth Diameter (mm)		Growth Inhibition Percentage (%)	
	A. alternata OR236467	*A. alternata* OR236468	OR236467	OR236468
Control (0 ppm)	78.35 ± 0.16 ^{a}	58.14 ± 0.29 ^{a}	0.00 ^{a}	0.00 ^{a}
50	55.17 ± 0.52 ^{b}	56.87 ± 0.58 ^{a}	29.58 ^{a}	2.18 ^{b}
100	41.34 ± 0.67 ^{c}	44.97 ± 0.41 ^{b}	47.24 ^{b}	22.65 ^{c}
200	34.51 ± 0.43 ^{d}	35.55 ± 0.22 ^{c}	55.95 ^{c}	38.85 ^{d}
400	26.84 ± 0.53 ^{e}	28.91 ± 0.34 ^{d}	65.74 ^{d}	50.28 ^{e}
800	18.89 ± 0.78 ^{f}	22.89 ± 0.78 ^{e}	75.89 ^{e}	60.63 ^{f}

Different letters in the same column indicated that values were significantly different at $p \leq 0.05$.

3.9. Antioxidant Activity

The DPPH inhibition percentages of the biogenic IONPs prepared using L. nobilis leaves, at concentrations ranging from 50 to 250 µg/mL, were found to range from 34.61% to 83.27%, respectively (Figure 12). In comparison, the DPPH inhibition percentages

of ascorbic acid ranged from 37.56% to 86.12%, respectively, for concentrations of 50 to 250 µg/mL, and the results of this investigation were consistent with the findings of a prior research [73]. Moreover, the detected IC_{50} value of the biogenic IONPs was found to be 122.57 µg/mL, whereas the standard ascorbic acid revealed IC_{50} of 108.21 µg/mL.

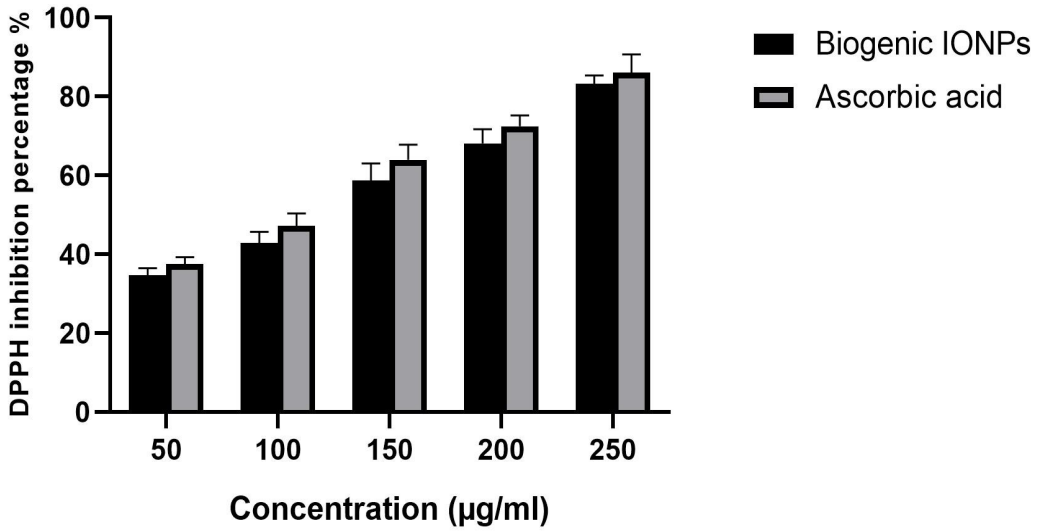

Figure 12. DPPH inhibition percentages (%) of the biogenic IONPs compared to the standard ascorbic acid.

4. Conclusions

Laurus nobilis leaf extract mediated the green biofabrication of the IONPs of potential physicochemical features. The biogenic IONPs were spherical in shape with an average particle size diameter of 46.312 ± 9.53 nm, whereas TEM analysis revealed the incorporation of the biosynthesized IONPs within a matrix-like structure which could be assigned to the capping biomolecules of the plant extract. The biogenic IONPs demonstrated potential antifungal efficacy against the tested fungal pathogens, indicating their potential application as biofungicides for the effective management of fungal phytopathogens, reducing reliance on chemical fungicides, which are harmful to the environment and human health. Furthermore, the biogenic IONPs displayed a higher antioxidant activity against the DPPH radical, indicating their potential suitability for biomedical applications.

Author Contributions: Conceptualization, M.T.Y. and A.A.A.-A.; methodology, M.T.Y.; software, M.T.Y.; validation, M.T.Y. and F.O.A.-O.; formal analysis, M.T.Y., A.A.A.-A. and F.O.A.-O.; investigation, M.T.Y. and R.I.A.; resources, A.A.A.-A.; data curation, M.T.Y.; writing—original draft preparation, M.T.Y.; writing—review and editing, M.T.Y., A.A.A.-A. and F.O.A.-O.; visualization, M.T.Y.; supervision, A.A.A.-A. and F.O.A.-O.; project administration, A.A.A.-A.; funding acquisition, M.T.Y. All authors have read and agreed to the published version of the manuscript.

Funding: This research was funded by the Researchers Supporting Project number (RSPD2023R1105), King Saud University, Riyadh, Saudi Arabia.

Institutional Review Board Statement: Not applicable.

Informed Consent Statement: Not applicable.

Data Availability Statement: Not applicable.

Acknowledgments: The authors extend their appreciation to the Researchers Supporting Project number (RSPD2023R1105), King Saud University, Riyadh, Saudi Arabia.

Conflicts of Interest: The authors declare no conflict of interest.

References

1. Dukare, A.S.; Paul, S.; Nambi, V.E.; Gupta, R.K.; Singh, R.; Sharma, K.; Vishwakarma, R.K. Exploitation of Microbial Antagonists for the Control of Postharvest Diseases of Fruits: A Review. *Crit. Rev. Food Sci. Nutr.* **2019**, *59*, 1498–1513. [CrossRef]
2. Carmona-Hernandez, S.; Reyes-Pérez, J.J.; Chiquito-Contreras, R.G.; Rincon-Enriquez, G.; Cerdan-Cabrera, C.R.; Hernandez-Montiel, L.G. Biocontrol of Postharvest Fruit Fungal Diseases by Bacterial Antagonists: A Review. *Agronomy* **2019**, *9*, 121. [CrossRef]
3. Fisher, M.C.; Henk, D.A.; Briggs, C.J.; Brownstein, J.S.; Madoff, L.C.; McCraw, S.L.; Gurr, S.J. Emerging Fungal Threats to Animal, Plant and Ecosystem Health. *Nature* **2012**, *484*, 186–194. [CrossRef]
4. Benedict, K.; Chiller, T.M.; Mody, R.K. Invasive Fungal Infections Acquired from Contaminated Food or Nutritional Supplements: A Review of the Literature. *Foodborne Pathog. Dis.* **2016**, *13*, 343–349. [CrossRef]
5. Leyva Salas, M.; Mounier, J.; Valence, F.; Coton, M.; Thierry, A.; Coton, E. Antifungal Microbial Agents for Food Biopreservation—A Review. *Microorganisms* **2017**, *5*, 37. [CrossRef] [PubMed]
6. Yuan, S.; Yan, J.; Wang, M.; Ding, X.; Zhang, Y.; Li, W.; Cao, J.; Jiang, W. Transcriptomic and Metabolic Profiling Reveals 'Green Ring' and 'Red Ring' on Jujube Fruit upon Postharvest Alternaria Alternata Infection. *Plant Cell Physiol.* **2019**, *60*, 844–861. [CrossRef] [PubMed]
7. Guo, W.; Fan, K.; Nie, D.; Meng, J.; Huang, Q.; Yang, J.; Shen, Y.; Tangni, E.K.; Zhao, Z.; Wu, Y.; et al. Development of a QuEChERS-Based UHPLC-MS/MS Method for Simultaneous Determination of Six Alternaria Toxins in Grapes. *Toxins* **2019**, *11*, 87. [CrossRef]
8. Shu, C.; Zhao, H.; Jiao, W.; Liu, B.; Cao, J.; Jiang, W. Antifungal Efficacy of Ursolic Acid in Control of Alternaria Alternata Causing Black Spot Rot on Apple Fruit and Possible Mechanisms Involved. *Sci. Hortic.* **2019**, *256*, 108636. [CrossRef]
9. Saha, D.; Fetzner, R.; Burkhardt, B.; Podlech, J.; Metzler, M.; Dang, H.; Lawrence, C.; Fischer, R. Identification of a Polyketide Synthase Required for Alternariol (AOH) and Alternariol-9-Methyl Ether (AME) Formation in Alternaria Alternata. *PLoS ONE* **2012**, *7*, e40564. [CrossRef]
10. Liu, Y.; Wang, Y.; Ma, L.; Fu, R.; Liu, H.; Cui, Y.; Zhao, Q.; Zhang, Y.; Jiao, B.; He, Y. A CRISPR/Cas12a-Based Photothermal Platform for the Portable Detection of Citrus-Associated Alternaria Genes Using a Thermometer. *Int. J. Biol. Macromol.* **2022**, *222*, 2661–2669. [CrossRef]
11. Shtienberg, D. Effects of Host Physiology on the Development of Core Rot, Caused by Alternaria Alternata, in Red Delicious Apples. *Phytopathology* **2012**, *102*, 769–778. [CrossRef]
12. Bai, Y.; Feng, Z.; Paerhati, M.; Wang, J. Phenylpropanoid Metabolism Enzyme Activities and Gene Expression in Postharvest Melons Inoculated with Alternaria Alternata. *Appl. Biol. Chem.* **2021**, *64*, 83. [CrossRef]
13. Castro, J.C.; Endo, E.H.; de Souza, M.R.; Zanqueta, E.B.; Polonio, J.C.; Pamphile, J.A.; Ueda-Nakamura, T.; Nakamura, C.V.; Dias Filho, B.P.; de Abreu Filho, B.A. Bioactivity of Essential Oils in the Control of Alternaria Alternata in Dragon Fruit (Hylocereus Undatus Haw.). *Ind. Crops Prod.* **2017**, *97*, 101–109. [CrossRef]
14. Wenneker, M.; Thomma, B.P.H.J. Latent Postharvest Pathogens of Pome Fruit and Their Management: From Single Measures to a Systems Intervention Approach. *Eur. J. Plant Pathol.* **2020**, *156*, 663–681. [CrossRef]
15. Rafiq, S.; Kaul, R.; Sofi, S.A.; Bashir, N.; Nazir, F.; Ahmad Nayik, G. Citrus Peel as a Source of Functional Ingredient: A Review. *J. Saudi Soc. Agric. Sci.* **2018**, *17*, 351–358. [CrossRef]
16. Zaller, J.G.; Brühl, C.A. Editorial: Non-Target Effects of Pesticides on Organisms Inhabiting Agroecosystems. *Front. Environ. Sci.* **2019**, *7*, 75.
17. Kanwar, V.S.; Sharma, A.; Srivastav, A.L.; Rani, L. Phytoremediation of Toxic Metals Present in Soil and Water Environment: A Critical Review. *Environ. Sci. Pollut. Res.* **2020**, *27*, 44835–44860. [CrossRef]
18. Rani, L.; Thapa, K.; Kanojia, N.; Sharma, N.; Singh, S.; Grewal, A.S.; Srivastav, A.L.; Kaushal, J. An Extensive Review on the Consequences of Chemical Pesticides on Human Health and Environment. *J. Clean. Prod.* **2021**, *283*, 124657. [CrossRef]
19. Gikas, G.D.; Parlakidis, P.; Mavropoulos, T.; Vryzas, Z. Particularities of Fungicides and Factors Affecting Their Fate and Removal Efficacy: A Review. *Sustainability* **2022**, *14*, 4056. [CrossRef]
20. Moraes Bazioli, J.; Belinato, J.R.; Costa, J.H.; Akiyama, D.Y.; Pontes, J.G.d.M.; Kupper, K.C.; Augusto, F.; de Carvalho, J.E.; Fill, T.P. Biological Control of Citrus Postharvest Phytopathogens. *Toxins* **2019**, *11*, 460. [CrossRef]
21. Santamarina, M.; Ibáñez, M.; Marqués, M.; Roselló, J.; Giménez, S.; Blázquez, M. Bioactivity of Essential Oils in Phytopathogenic and Post-Harvest Fungi Control. *Nat. Prod. Res.* **2017**, *31*, 2675–2679. [CrossRef]
22. Elmer, W.; Ma, C.; White, J. Nanoparticles for Plant Disease Management. *Curr. Opin. Environ. Sci. Health* **2018**, *6*, 66–70. [CrossRef]
23. Singh, R.P.; Handa, R.; Manchanda, G. Nanoparticles in Sustainable Agriculture: An Emerging Opportunity. *J. Control. Release* **2021**, *329*, 1234–1248. [CrossRef]
24. Bandala, E.R.; Berli, M. Engineered Nanomaterials (ENMs) and Their Role at the Nexus of Food, Energy, and Water. *Mater. Sci. Energy Technol.* **2019**, *2*, 29–40. [CrossRef]
25. Ashraf, S.A.; Siddiqui, A.J.; Elkhalifa, A.E.O.; Khan, M.I.; Patel, M.; Alreshidi, M.; Moin, A.; Singh, R.; Snoussi, M.; Adnan, M. Innovations in Nanoscience for the Sustainable Development of Food and Agriculture with Implications on Health and Environment. *Sci. Total Environ.* **2021**, *768*, 144990. [CrossRef]

26. Zaytseva, O.; Neumann, G. Carbon Nanomaterials: Production, Impact on Plant Development, Agricultural and Environmental Applications. *Chem. Biol. Technol. Agric.* **2016**, *3*, 17. [CrossRef]
27. Vinzant, K.; Rashid, M.; Khodakovskaya, M.V. Advanced Applications of Sustainable and Biological Nano-Polymers in Agricultural Production. *Front. Plant Sci.* **2023**, *13*, 1081165. [PubMed]
28. El-Beltagi, H.S.; Bendary, E.S.; Ramadan, K.M.A.; Mohamed, H.I. Metallic Nanoparticles and Nano-Based Bioactive Formulations as Nano-Fungicides for Sustainable Disease Management in Cereals. In *Cereal Diseases: Nanobiotechnological Approaches for Diagnosis and Management*; Abd-Elsalam, K.A., Mohamed, H.I., Eds.; Springer Nature: Singapore, 2022; pp. 315–343, ISBN 978-981-19312-0-8.
29. Tesser, M.E.; Guilger, M.; Bilesky-José, N.; Risso, W.E.; de Lima, R.; dos Reis Martinez, C.B. Biogenic Metallic Nanoparticles (Ag, TiO_2, Fe) as Potential Fungicides for Agriculture: Are They Safe for the Freshwater Mussel Anodontites Trapesialis? *Chemosphere* **2022**, *309*, 136664. [CrossRef] [PubMed]
30. Ul Haq, I.; Ijaz, S. Use of Metallic Nanoparticles and Nanoformulations as Nanofungicides for Sustainable Disease Management in Plants. In *Nanobiotechnology in Bioformulations*; Prasad, R., Kumar, V., Kumar, M., Choudhary, D., Eds.; Nanotechnology in the Life Sciences; Springer International Publishing: Cham, Switzerland, 2019; pp. 289–316, ISBN 978-3-030-17061-5.
31. Hernández-Díaz, J.A.; Garza-García, J.J.; Zamudio-Ojeda, A.; León-Morales, J.M.; López-Velázquez, J.C.; García-Morales, S. Plant-Mediated Synthesis of Nanoparticles and Their Antimicrobial Activity against Phytopathogens. *J. Sci. Food Agric.* **2021**, *101*, 1270–1287. [CrossRef] [PubMed]
32. Maity, D.; Gupta, U.; Saha, S. Biosynthesized Metal Oxide Nanoparticles for Sustainable Agriculture: Next-Generation Nanotechnology for Crop Production, Protection and Management. *Nanoscale* **2022**, *14*, 13950–13989. [CrossRef]
33. Bilal, M.; Iqbal, H.M.N.; Adil, S.F.; Shaik, M.R.; Abdelgawad, A.; Hatshan, M.R.; Khan, M. Surface-Coated Magnetic Nanostructured Materials for Robust Bio-Catalysis and Biomedical Applications—A Review. *J. Adv. Res.* **2022**, *38*, 157–177. [CrossRef]
34. Abdelhamid, H.N.; Wu, H.-F. Multifunctional Graphene Magnetic Nanosheet Decorated with Chitosan for Highly Sensitive Detection of Pathogenic Bacteria. *J. Mater. Chem. B* **2013**, *1*, 3950. [CrossRef]
35. Gopal, J.; Abdelhamid, H.N.; Hua, P.-Y.; Wu, H.-F. Chitosan Nanomagnets for Effective Extraction and Sensitive Mass Spectrometric Detection of Pathogenic Bacterial Endotoxin from Human Urine. *J. Mater. Chem. B* **2013**, *1*, 2463–2475. [CrossRef]
36. Tartaj, P.; Morales, M.P.; González-Carreño, T.; Veintemillas-Verdaguer, S.; Serna, C.J. Advances in Magnetic Nanoparticles for Biotechnology Applications. *J. Magn. Magn. Mater.* **2005**, *290–291*, 28–34. [CrossRef]
37. Wani, A.H.; Amin, M.; Shahnaz, M.; Shah, M.A. Antimycotic Activity of Nanoparticles of MgO, FeO and ZnO on Some Pathogenic Fungi. *Int. J. Manuf. Mater. Mech. Eng.* **2012**, *2*, 59–70. [CrossRef]
38. Bilesky-José, N.; Maruyama, C.; Germano-Costa, T.; Campos, E.; Carvalho, L.; Grillo, R.; Fraceto, L.F.; de Lima, R. Biogenic α-Fe_2O_3 Nanoparticles Enhance the Biological Activity of Trichoderma against the Plant Pathogen Sclerotinia Sclerotiorum. *ACS Sustain. Chem. Eng.* **2021**, *9*, 1669–1683. [CrossRef]
39. Henam, S.D.; Ahmad, F.; Shah, M.A.; Parveen, S.; Wani, A.H. Microwave Synthesis of Nanoparticles and Their Antifungal Activities. *Spectrochim. Acta. A. Mol. Biomol. Spectrosc.* **2019**, *213*, 337–341. [CrossRef]
40. Bharathi, D.; Preethi, S.; Abarna, K.; Nithyasri, M.; Kishore, P.; Deepika, K. Bio-Inspired Synthesis of Flower Shaped Iron Oxide Nanoparticles (FeONPs) Using Phytochemicals of Solanum Lycopersicum Leaf Extract for Biomedical Applications. *Biocatal. Agric. Biotechnol.* **2020**, *27*, 101698. [CrossRef]
41. Mirza, A.U.; Kareem, A.; Nami, S.A.A.; Khan, M.S.; Rehman, S.; Bhat, S.A.; Mohammad, A.; Nishat, N. Biogenic Synthesis of Iron Oxide Nanoparticles Using Agrewia Optiva and Prunus Persica Phyto Species: Characterization, Antibacterial and Antioxidant Activity. *J. Photochem. Photobiol. B* **2018**, *185*, 262–274. [CrossRef]
42. Falade, A.O.; Adewole, K.E.; Adekola, A.-R.O.; Ikokoh, H.A.; Okaiyeto, K.; Oguntibeju, O.O. Aqueous Extract of Bay Leaf (Laurus Nobilis) Ameliorates Testicular Toxicity Induced by Aluminum Chloride in Rats. *Vet. World* **2022**, *15*, 2525. [CrossRef]
43. Afzal, S.; Sharma, D.; Singh, N.K. Eco-Friendly Synthesis of Phytochemical-Capped Iron Oxide Nanoparticles as Nano-Priming Agent for Boosting Seed Germination in Rice (*Oryza sativa* L.). *Environ. Sci. Pollut. Res.* **2021**, *28*, 40275–40287. [CrossRef]
44. Groiss, S.; Selvaraj, R.; Varadavenkatesan, T.; Vinayagam, R. Structural Characterization, Antibacterial and Catalytic Effect of Iron Oxide Nanoparticles Synthesised Using the Leaf Extract of Cynometra Ramiflora. *J. Mol. Struct.* **2017**, *1128*, 572–578. [CrossRef]
45. Jagathesan, G.; Rajiv, P. Biosynthesis and Characterization of Iron Oxide Nanoparticles Using Eichhornia Crassipes Leaf Extract and Assessing Their Antibacterial Activity. *Biocatal. Agric. Biotechnol.* **2018**, *13*, 90–94. [CrossRef]
46. Braim, F.S.; Nik Ab Razak, N.N.A.; Aziz, A.A.; Dheyab, M.A.; Ismael, L.Q. Rapid Green-Assisted Synthesis and Functionalization of Superparamagnetic Magnetite Nanoparticles Using Sumac Extract and Assessment of Their Cellular Toxicity, Uptake, and Anti-Metastasis Property. *Ceram. Int.* **2023**, *49*, 7359–7369. [CrossRef]
47. Periakaruppan, R.; Chen, X.; Thangaraj, K.; Jeyaraj, A.; Nguyen, H.H.; Yu, Y.; Hu, S.; Lu, L.; Li, X. Utilization of Tea Resources with the Production of Superparamagnetic Biogenic Iron Oxide Nanoparticles and an Assessment of Their Antioxidant Activities. *J. Clean. Prod.* **2021**, *278*, 123962. [CrossRef]
48. Hoffmann, N.; Tortella, G.; Hermosilla, E.; Fincheira, P.; Diez, M.C.; Lourenço, I.M.; Seabra, A.B.; Rubilar, O. Comparative Toxicity Assessment of Eco-Friendly Synthesized Superparamagnetic Iron Oxide Nanoparticles (SPIONs) in Plants and Aquatic Model Organisms. *Minerals* **2022**, *12*, 451. [CrossRef]
49. Alghuthaymi, M.A.; Rajkuberan, C.; Santhiya, T.; Krejcar, O.; Kuča, K.; Periakaruppan, R.; Prabukumar, S. Green Synthesis of Gold Nanoparticles Using Polianthes Tuberosa L. Floral Extract. *Plants* **2021**, *10*, 2370. [CrossRef] [PubMed]

50. Selim, Y.A.; Azb, M.A.; Ragab, I.; HM Abd El-Azim, M. Green Synthesis of Zinc Oxide Nanoparticles Using Aqueous Extract of Deverra Tortuosa and Their Cytotoxic Activities. *Sci. Rep.* **2020**, *10*, 3445. [CrossRef] [PubMed]
51. Shehzad, A.; Qureshi, M.; Jabeen, S.; Ahmad, R.; Alabdalall, A.H.; Aljafary, M.A.; Al-Suhaimi, E. Synthesis, Characterization and Antibacterial Activity of Silver Nanoparticles Using Rhazya Stricta. *PeerJ* **2018**, *6*, e6086. [CrossRef] [PubMed]
52. Nagaonkar, D.; Gaikwad, S.; Rai, M. Catharanthus Roseus Leaf Extract-Synthesized Chitosan Nanoparticles for Controlled in Vitro Release of Chloramphenicol and Ketoconazole. *Colloid Polym. Sci.* **2015**, *293*, 1465–1473. [CrossRef]
53. Umashankari, J.; Inbakandan, D.; Ajithkumar, T.T.; Balasubramanian, T. Mangrove Plant, Rhizophora Mucronata (Lamk, 1804) Mediated One Pot Green Synthesis of Silver Nanoparticles and Its Antibacterial Activity against Aquatic Pathogens. *Aquat. Biosyst.* **2012**, *8*, 11. [CrossRef] [PubMed]
54. Vijayan, R.; Joseph, S.; Mathew, B. Green Synthesis of Silver Nanoparticles Using Nervalia Zeylanica Leaf Extract and Evaluation of Their Antioxidant, Catalytic, and Antimicrobial Potentials. *Part. Sci. Technol.* **2019**, *37*, 809–819. [CrossRef]
55. Chakraborty, A.; Sarangapany, S.; Mishra, U.; Mohanty, K. Green Synthesized Magnetically Separable Iron Oxide Nanoparticles for Efficient Heterogeneous Photo-Fenton Degradation of Dye Pollutants. *J. Clust. Sci.* **2022**, *33*, 675–685. [CrossRef]
56. Sharmila, G.; Thirumarimurugan, M.; Muthukumaran, C. Green Synthesis of ZnO Nanoparticles Using Tecoma Castanifolia Leaf Extract: Characterization and Evaluation of Its Antioxidant, Bactericidal and Anticancer Activities. *Microchem. J.* **2019**, *145*, 578–587. [CrossRef]
57. Donga, S.; Bhadu, G.R.; Chanda, S. Antimicrobial, Antioxidant and Anticancer Activities of Gold Nanoparticles Green Synthesized Using Mangifera Indica Seed Aqueous Extract. *Artif. Cells Nanomed. Biotechnol.* **2020**, *48*, 1315–1325. [CrossRef]
58. Demirezen, D.A.; Yılmaz, Ş.; Yılmaz, D.D.; Yıldız, Y.Ş. Green Synthesis of Iron Oxide Nanoparticles Using Ceratonia Siliqua L. Aqueous Extract: Improvement of Colloidal Stability by Optimizing Synthesis Parameters, and Evaluation of Antibacterial Activity against Gram-Positive and Gram-Negative Bacteria. *Int. J. Mater. Res.* **2022**, *113*, 849–861. [CrossRef]
59. Ilmetov, R. Photocatalytic Activity of Hematite Nanoparticles Prepared by Sol-Gel Method. *Mater. Today Proc.* **2019**, *6*, 11–14. [CrossRef]
60. Rajendran, K.; Karunagaran, V.; Mahanty, B.; Sen, S. Biosynthesis of Hematite Nanoparticles and Its Cytotoxic Effect on HepG2 Cancer Cells. *Int. J. Biol. Macromol.* **2015**, *74*, 376–381. [CrossRef]
61. Joshi, D.P.; Pant, G.; Arora, N.; Nainwal, S. Effect of Solvents on Morphology, Magnetic and Dielectric Properties of (α-Fe_2O_3 @SiO_2) Core-Shell Nanoparticles. *Heliyon* **2017**, *3*, e00253. [CrossRef] [PubMed]
62. Alikord, M.; Shariatifar, N.; Saraji, M.; Jahed Khaniki, G.; Hosseini, H.; Fazeli, M. Biosynthesis of Zinc Oxide Nanoparticles Using Fermented Table Olive Extract: A Novel and Green Approach with Potential Applications. *BioNanoScience* **2023**, *13*, 1036–1051. [CrossRef]
63. Iqbal, J.; Abbasi, B.A.; Ahmad, R.; Shahbaz, A.; Zahra, S.A.; Kanwal, S.; Munir, A.; Rabbani, A.; Mahmood, T. Biogenic Synthesis of Green and Cost Effective Iron Nanoparticles and Evaluation of Their Potential Biomedical Properties. *J. Mol. Struct.* **2020**, *1199*, 126979. [CrossRef]
64. Haris, M.; Fatima, N.; Iqbal, J.; Chalgham, W.; Mumtaz, A.S.; El-Sheikh, M.A.; Tavafoghi, M. *Oscillatoria limnetica* Mediated Green Synthesis of Iron Oxide (Fe_2O_3) Nanoparticles and Their Diverse In Vitro Bioactivities. *Molecules* **2023**, *28*, 2091. [CrossRef] [PubMed]
65. Periakaruppan, R.; Kumar, T.S.; Vanathi, P.; Al-Awsi, G.R.L.; Al-Dayan, N.; Dhanasekaran, S. Phyto-Synthesis and Characterization of Parthenium-Mediated Iron Oxide Nanoparticles and an Evaluation of Their Antifungal and Antioxidant Activities and Effect on Seed Germination. *JOM* **2023**, 1–8. [CrossRef]
66. Win, T.T.; Khan, S.; Bo, B.; Zada, S.; Fu, P. Green Synthesis and Characterization of Fe_3O_4 Nanoparticles Using Chlorella-K01 Extract for Potential Enhancement of Plant Growth Stimulating and Antifungal Activity. *Sci. Rep.* **2021**, *11*, 21996. [CrossRef]
67. Jamzad, M.; Kamari Bidkorpeh, M. Green Synthesis of Iron Oxide Nanoparticles by the Aqueous Extract of Laurus Nobilis L. Leaves and Evaluation of the Antimicrobial Activity. *J. Nanostructure Chem.* **2020**, *10*, 193–201. [CrossRef]
68. Ahmad, W.; Kumar Jaiswal, K.; Amjad, M. Euphorbia Herita Leaf Extract as a Reducing Agent in a Facile Green Synthesis of Iron Oxide Nanoparticles and Antimicrobial Activity Evaluation. *Inorg. Nano-Met. Chem.* **2021**, *51*, 1147–1154. [CrossRef]
69. Cruz-Luna, A.R.; Cruz-Martínez, H.; Vásquez-López, A.; Medina, D.I. Metal Nanoparticles as Novel Antifungal Agents for Sustainable Agriculture: Current Advances and Future Directions. *J. Fungi* **2021**, *7*, 1033. [CrossRef] [PubMed]
70. Malandrakis, A.A.; Kavroulakis, N.; Chrysikopoulos, C.V. Metal Nanoparticles against Fungicide Resistance: Alternatives or Partners? *Pest Manag. Sci.* **2022**, *78*, 3953–3956. [CrossRef] [PubMed]
71. Cruz-Luna, A.R.; Vásquez-López, A.; Rojas-Chávez, H.; Valdés-Madrigal, M.A.; Cruz-Martínez, H.; Medina, D.I. Engineered Metal Oxide Nanoparticles as Fungicides for Plant Disease Control. *Plants* **2023**, *12*, 2461. [CrossRef] [PubMed]
72. Alam, T.; Akbar, F.; Ali, M.; Munis, M.F.H.; Khan, J. Biosynthesis of iron oxide nanoparticles via crocus sativus and their antifungal efficacy against verticillium wilt pathogen verticillium dahliae. *BioRxiv* **2019**, 861401. [CrossRef]
73. Singh, K.; Chopra, D.S.; Singh, D.; Singh, N. Optimization and Ecofriendly Synthesis of Iron Oxide Nanoparticles as Potential Antioxidant. *Arab. J. Chem.* **2020**, *13*, 9034–9046. [CrossRef]